Cosserat elasticity of octet truss titanium alloy lattices

September 12, 2023

K. Goyal, Z. Rueger, E. Davis and R. S. Lakes, Cosserat elasticity of octet truss titanium alloy lattices, Journal of Mechanics of Materials and Structures, 16 (5) 645-654 (2021). https://doi.org/10.2140/jomms.2021.16.645

Abstract

The octet truss lattice is known to be stretch dominated and to offer superior mechanical properties compared with foams of identical (low) density and solid composition. In the lattices, size effects in effective modulus were observed; they were of small magnitude, 30% in torsion and 10% in bending. The Cosserat characteristic lengths in torsion (1 mm) and in bending (0.5 mm) are considerably smaller than the cell size, 4.5 mm. The lattice is therefore considered to be weakly Cosserat elastic in comparison with designed lattices for which size effects can exceed a factor of 30, and also in comparison with foams for which size effects can exceed a factor of 8.

1 Introduction and rationale

Pure titanium has a density of 4.5 g/cc and a Young's modulus of 116 GPa. Various titanium alloys are in widespread use. Ti5553 is considered to be a relatively new high performance alloy. It is a titanium alloy that has been prepared by laser metal deposition for aerospace applications [1]. It has also been prepared via additive manufacturing [2]. The Ti-5553 alloy, also known as 5Al-5Mo-5V-3Cr, has a reported tensile strength up to 1309 MPa with more than 10% elongation [3]. The quoted density [4] is 4.6 g/cc.

Reduced density can be achieved by making a foam or a lattice from a solid material. Lattices, in contrast to foams, are periodic arrays of structural elements. If the structural elements are ribs, the lattice is called a rib lattice or a truss lattice. In a simple cubic rib lattice, one third of the ribs are aligned with forces applied in principal directions, so via a Voigt analysis, the lattice Young's modulus E is $\frac{E}{E_s} = \frac{1}{3} [\frac{\rho}{\rho_s}]$ with ρ as the lattice density and ρ_s as the density of the solid and E_s as the solid modulus. Properties in oblique directions are much lower because the ribs then bend rather than stretching or compressing axially. The simple cubic rib lattice is highly anisotropic. Elastic isotropy in a lattice can be achieved by combining ribs of a simple cubic lattice with oblique ribs of a body centered lattice. For an elastically isotropic rib lattice [6] [7], $\frac{E}{E_s} = \frac{1}{6} [\frac{\rho}{\rho_s}]$.

The octet truss lattice was envisaged by Buckminster Fuller [8] in 1967 in the context of large scale building construction. It contains regular octahedra with regular tetrahedra in a repeating array that can be obtained from a face-centered-cubic (FCC) lattice by connecting the nearest-neighbor lattice sites. The octet truss lattice has cubic symmetry and it is elastically anisotropic with three independent elastic constants. In principal directions, the Young's modulus E via analysis is

$$\frac{E}{E_s} = \frac{1}{9} \left[\frac{\rho}{\rho_s} \right] \tag{1}$$

in which E_s is Young's modulus of the solid from which the lattice is made, ρ is the lattice density and ρ_s is the density of the solid [9]. The shear modulus is $J_{44}^{-1} = G = \frac{1}{12} \frac{\rho}{\rho_s} E_s$. One can obtain higher E in oblique directions than in principal directions, at the expense of stretch - shear coupling effects and a smaller shear modulus. The first power in the density indicates a stretch dominated lattice which cannot deform without stretching or compressing the ribs. By contrast, foams or lattices with cells in the shape of truncated octahedra (tetrakaidecahedra) are bend dominated and are much less stiff at low density,

$$\frac{E}{E_s} \approx \left[\frac{\rho}{\rho_s}\right]^2. \tag{2}$$

Rib lattices have long been known in the context of analytical mechanics; recently they have been explored in detail because they can be made via additive manufacturing techniques.

Materials with microstructure have been observed to deviate from the predictions of classical elasticity when the structure size is non-negligible in comparison with length scales associated with the experiment. Behavior has been observed to follow Cosserat elasticity which contains more freedom than classical elasticity. The rationale for considering a generalized continuum theory for lattice materials is to attain greater predictive power than is possible via classical elasticity. Also, Cosserat solids exhibit lower stress concentration factors [10] around holes and notches than classical elastic solids.

Rib lattices based on titanium alloy as well as solid rods of the same alloy are examined in the present study. Lattice specimens had square cross section.

2 Methods

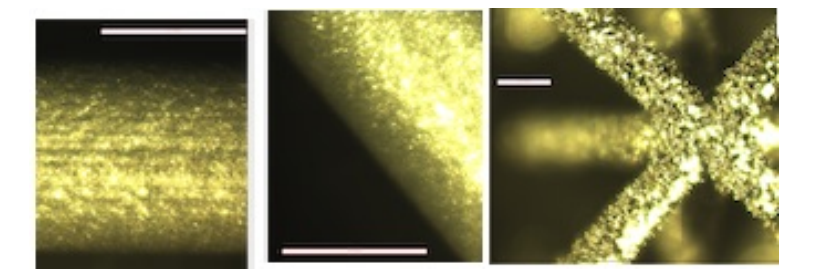


Figure 1: Optical micrographs of alloy specimens. Left, 0° ; scale bar 5 mm. Center 90° ; scale bar 5 mm. Right, lattice; scale bar 0.5 mm.

Specimens were designated Ti5553 191-A0331. The specimens as received were gray in color. Solid specimens were rods designated 0°, 45°, and 90°; they were 6.504 mm in diameter and 50 mm

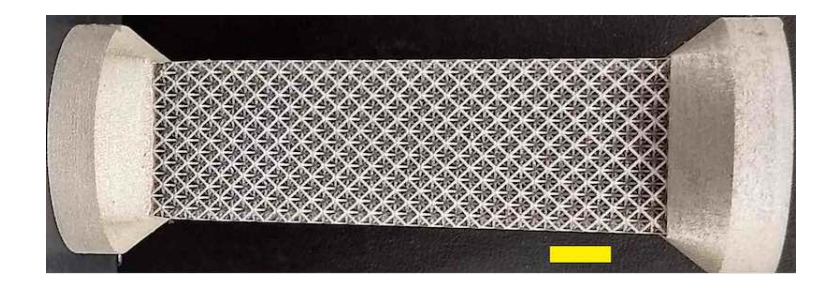


Figure 2: Lattice specimen seven cells across. Scale bar, 1 cm.

long with the exception of the 0° specimen which had a longitudinal flat. Specimens had a surface texture from the 3D printing as shown in Figure 1.

An Additive Industries (AI) MetalFAB1 laser powder bed fusion (LPBF) system processing Titanium-5Al-5Mo-5V-3Cr, Ti-5553, manufactured the lattice specimens. The AI MetalFAB1 employs four full-field Ytterbium (Yb) doped fiber lasers (maximum power $P_{max} = 500$ W, wavelength $\lambda = 1070$ nm, and spot size 100 - 105 μ m) to build parts with a continuous wave exposure strategy. The lattice portion and solid bases of each part were fabricated using previously developed build parameters. Laser power ranged from 120 to 160 W within both the lattice and base volumes while laser speed ranged from 600 to 950 mm/s depending on geometry. Layer thickness was constant at 40 μ m. All parts were printed such that their longitudinal axes were perpendicular to the surface of the build plate. Each build layer was consolidated by the lasers using scan path striping. Scan path striping is a laser scanning strategy that divides the area to be consolidated into smaller sets of laser raster vectors. Each build layer was rotated 67 degrees to avoid stacking of scan corners and interior seams. The specimens were then removed via wire-electrical discharge machining.

Preliminary ultrasonic experiments on solid material were done using Panametrics 1 MHz broadband longitudinal and shear transducers excited by a Tektronix AFG 3051c arbitrary function generator set in burst mode for bursts of sinusoids. Bursts from one to five cycles were explored; a burst of one cycle was used in the experiments reported. Input and output signals were observed using a Tektronix DPO 3014 digital oscilloscope. Frequency was varied in steps from 100 kHz to 1 MHz: 100 kHz, 200 kHz, 500 kHz, 1 MHz, 10 MHz.

Rib lattices of different size were studied. They had a cell size $L_c = 4.5$ mm in principal directions. The ribs visible at the surface were at an angle 45° with respect to principal directions and had a length $L_r = L_c/\sqrt{2}$. Rib thickness w_r was about 0.53 mm. The lattices had octet structure and were from two to seven cells wide in square cross section. The lattices were provided with end pieces for attachment to test devices as shown in Figure 2. Lattice density was determined by cutting the end pieces off one specimen following mechanical testing and measuring mass and dimensions.

Quasi-static experiments were done in torsion and in bending using a broadband viscoelastic spectroscopy instrument (BVS) at a frequency of 1 Hz. The BVS was originally designed to perform viscoelastic measurements over a wide range of frequency from slow tests limited by the experimenter's patience to resonant studies at 100 kHz or more [11]. To that end, inertia was minimized and parasitic damping and phase angles were minimized. Torque was applied via an electric current from a SRS DS345 function generator through a Helmholtz coil acting upon a high intensity magnet cemented to the specimen. Angular displacement was measured via a laser beam reflected from a mirror attached to the specimen upon a position sensitive silicon detector. The specimen was supported from above rather than from below to allow for highly compliant specimens

of rubber or foam which could buckle under their own weight. The support rod is steel, 25.4 mm in diameter, fixed to a brass top plate 2.5 cm thick. The BVS instrument enclosure is a massive brass hollow cylinder of outer radius 8.8 cm with walls more than 1.2 cm thick, supported by a vibration isolator. The instrument was covered with a clear polymer enclosure to eliminate disturbance from air currents during tests. The instrument was intended for viscoelastic measurements on metal alloy specimens 3 mm in diameter and 15 to 30 mm long or polymers or compliant foam. The BVS provided more than adequate structural stiffness for these specimens; the structural rigidity of the instrument exceeds that of such specimens by many orders of magnitude. For such specimens, the fundamental natural frequency can be several kilohertz, and higher modes are accessible.

Recently the BVS instrument was used for larger and stiffer specimens of lattices because it has the capability of torsion and pure bending tests on the same specimen. If the specimen has too large a structural rigidity, instrument compliance must be evaluated and if necessary, compensated.

To that end, differential rotation measurement was achieved by measuring rotation using two mirrors attached to different locations on the specimen. Subtraction of the rotations provides the desired differential rotation. Because the BVS has one port for the laser beam, mirrors were placed on stalks. Use of a stalk limits the measurements to low frequency because the stalk can resonate in bending. Stalks were made of aluminum alloy rather than PMMA polymer so that they are stiffer and have a higher natural frequency.

Signals from the light detector were sufficiently small that signal averaging was used on a Tektronix TDS3014 B digital oscilloscope. For all tests, a SRS 560 preamplifier was used. A band pass was set such that only frequencies between 0.03 Hz and 300 Hz were allowed, to reduce noise. The filter was turned off during calibration to prevent the preamplifier from filtering out the quasi - DC signal used for calibration. Multiple tests were done and the results were averaged. Some tests were repeated after demounting and remounting the specimen.

Frequency dependence of the setup was tested. It was verified that the stalk natural frequencies were well above the test frequency of 1 Hz.

The effective moduli were plotted vs. specimen width. The torsion and bending results were curve fitted using Cosserat elasticity.

3 Analysis

The constitutive equations for linear isotropic Cosserat [12] elasticity are:

$$\sigma_{ij} = 2G\epsilon_{ij} + \lambda \epsilon_{kk} \delta_{ij} + \kappa e_{ijk} (r_k - \phi_k) \tag{3}$$

$$m_{ij} = \alpha \phi_{k,k} \delta_{ij} + \beta \phi_{i,j} + \gamma \phi_{j,i}. \tag{4}$$

Cosserat solids that admit local inertia are called micropolar [13]. The points in a Cosserat solid have rotational freedom ϕ_k , called micro-rotation. This local rotation in general differs from $r_k = \frac{1}{2}e_{klm}u_{m,l}$ which is the "macro" rotation based on the antisymmetric part of gradient of displacement u_i . e_{ijk} is the permutation symbol. The Cauchy stress σ_{ij} (force per unit area) in Cosserat elasticity can be asymmetric, in contrast to classical elasticity in which the stress is symmetric. Cosserat theory includes a couple stress m_{ij} (a torque per unit area) which balances the distributed moment from the asymmetric stress.

Cosserat elasticity admits six elastic constants for isotropic materials. These are λ , G, α , β , γ , κ . Constants λ and G have the same meaning as in classical elasticity. G is the shear modulus in the absence of gradients. Constants α , β , γ provide sensitivity to rotation gradient. The Cosserat constant κ quantifies the coupling between local rotation ϕ_k and the rotation r_k associated with displacement gradients. The characteristic length for torsion is defined as $\ell_t = \sqrt{\frac{\beta+\gamma}{2G}}$. The

characteristic length for bending is defined as $\ell_b = \sqrt{\frac{\gamma}{4G}}$. The dimensionless coupling number is defined as $N = \sqrt{\frac{\kappa}{2G + \kappa}}$.

For a round sotropic Cosserat rod in torsion, an exact solution is available for interpreting experiments [14]. In the regime N=1, $\frac{M}{\theta}=G[\frac{\pi}{2}r^4](1+6(\frac{\ell_t}{r})^2)$. G is the true shear modulus in the absence of gradients; r is the radius. M is the applied moment and θ is the twist angle per length. The rigidity ratio Ω , the ratio of observed structural rigidity to the asymptotic value at large radius, is

$$\Omega = 1 + 6\left(\frac{\ell_t}{r}\right)^2. \tag{5}$$

The torsion size effect analysis for a square bar [15] expressed in terms of the bar half width a is rather complicated. The size effect relation simplifies considerably if one assumes $\ell_t \ll w$ and $\ell_b = \frac{1}{2}\ell_t$. The rigidity ratio Ω in terms of the bar full width w = 2a is, with M as the applied torque and θ as the twist angle per length,

$$\Omega = \frac{M}{\frac{898}{399}Ga^4\theta} = 1 + 28.4(\frac{\ell_t}{w})^2. \tag{6}$$

The bending size effect analysis for a square bar [16] is also complicated but it simplifies considerably if $\beta/\gamma = -\nu$. The rigidity ratio Ω , with w as the bar full width, is then, with ν as Poisson's ratio,

$$\Omega = 1 + 24(\frac{\ell_b}{w})^2 (1 - \nu). \tag{7}$$

This relation is similar to the relation Eq. (5) for the round bar size effect. This equation also corresponds to the exact solution obtained for bending of a plate to a cylindrical shape [14]. The physical meaning of the characteristic length is the size scale at which deviations from classical elasticity are predicted to become prominent.

As for the relation between the characteristic lengths in isotropic materials, at the upper limit $\frac{\beta}{\gamma} = 1$, $\ell_b = \frac{1}{2}\ell_t$; for $\frac{\beta}{\gamma} = 0$, $\ell_b = \frac{1}{\sqrt{2}}\ell_t$, and for $\frac{\beta}{\gamma} \to -1$, $\ell_b >> \ell_t$.

If the material is anisotropic, the characteristic lengths as well as the Young's and shear moduli may be considered as technical constants; the usual isotropic interrelations between elastic constants do not apply.

4 Results and discussion

4.1 Solid properties

In the ultrasonic experiments on the solid material, the pulse time delay was essentially independent of frequency from 100 kHz to 1 MHz. Time resolution is superior at higher frequency but the signal amplitude and signal quality decreased with increase in frequency. Time delay measurements taken at 100 kHz indicate a Young's modulus about 80 GPa within only one significant figure. Precision was limited by the wave period in comparison with the time delay. Signal quality was insufficient at 1 MHz and at 10 MHz to allow meaningful measurements. At 100 kHz, the wavelength $\lambda = 42$ mm. For these lower frequencies, the wavelength is considerably longer than the specimen diameter 6 mm so the interpretation is that the wave speed reveals Young's modulus E not the tensorial modulus C_{11} .

Table 1: Ti5553 solid titanium alloy properties: density and moduli via BVS.

Specimen	ρ (g/cc)	E(GPa)	G(GPa)
0°	-	$\geq 86, 74$	≥ 20
45°	4.8	76	27
90°	4.5	89	27

Solid material properties via BVS are as follows. The 45° solid specimen with a round cross section exhibited a shear modulus G=27 GPa and a Young's modulus E=76 GPa; the 90° solid specimen with a round cross section exhibited a shear modulus G=27 GPa and a Young's modulus E=89 GPa. For the 0° solid specimen $G\geq 20$ GPa and $E\geq 86$ GPa and $E\geq 74$ GPa depending on the orientation of the cut out flat. Moduli are reported as greater than because the specimens were assumed to be perfectly round. Table 1 shows density and moduli for three solid specimens.

As for comparison with prior measurements, moduli for Ti5553 alloys have been reported to vary with preparation methods [5]. For bimodal alloy, Young's modulus is E=110 GPa; for beta alloy, E=69 GPa. The designations refer to microstructure. In the present results, Young's moduli for the provided specimens are between those extremes. The present specimens have been made by additive manufacturing and that adds at least two more variables associated with porosity and orientation.

4.2 Lattice elastic properties

The lattice density was found to be 0.534 g/cm³, so since titanium has a density of 4.6 g/cc, the density divided by the density of the solid is $\frac{\rho}{\rho_s} = 0.116$. So if the solid modulus is 80 GPa, the theoretical lattice Young's modulus E via Eq. (1) is 1.03 GPa compared with observed $E_0 = 0.93$ GPa. This is considered satisfactory agreement in view of the experimental variance and possible variance due to 3D printing. Details of the 3D print pattern of the ribs are not known. For a foam of the same relative density and solid material, E = 1.13 GPa, similar to the lattice and G = 0.44 GPa, 61% that of the lattice. For lower density, the lattice would have much higher moduli than the foam.

The ratio of Young's modulus to shear modulus was 1.31, compared with a value 1.33 from theory [9]. This is also considered satisfactory agreement in view of the experimental variance and possible variance due to 3D printing.

4.3 Size effects and interpretation

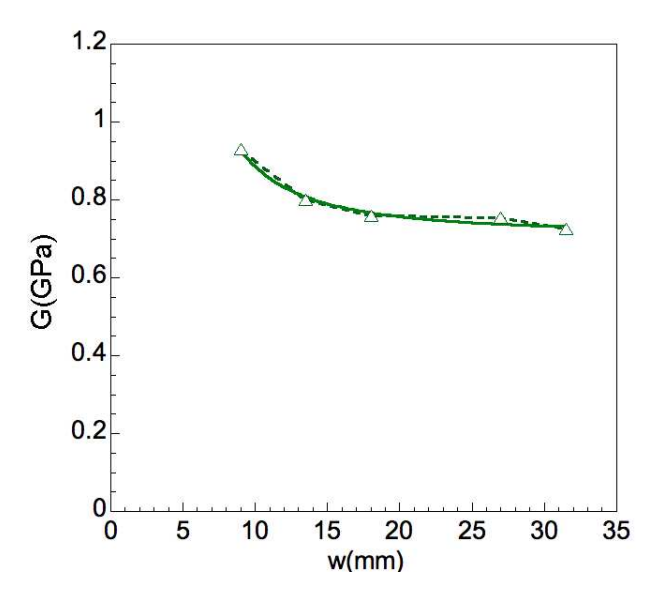


Figure 3: Shear modulus G vs. width w for the octet truss lattice. Points are experimental. The solid green curve is a curve fit to the torsion results.

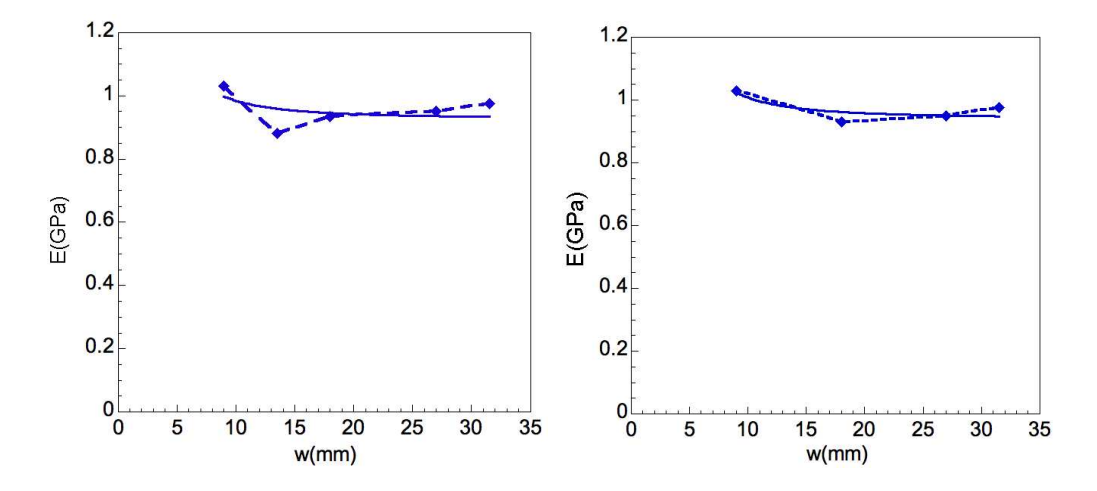


Figure 4: Young's modulus E vs. width w for the octet truss lattice. Points are experimental. The solid curve is a curve fit to the bending results. Left plot: all results; right plot, fit with low point excluded.

The instrument structural rigidity was sufficiently high that the largest lattice specimen required only a 6% or less correction from the differential angle measurement.

Lattice rigidity vs. specimen size discloses size effects in shear modulus as shown in Figure 3 and in Young's modulus as shown in Figure 4. Size effects were of relatively small magnitude, 30% in torsion and 10% in bending. If the lattice were classically elastic, the inferred moduli would be independent of specimen size.

A curve fit (solid green curve) for the torsion results using Eq. (5) revealed the following elastic constants. The inferred asymptotic shear modulus was $G_0 = 0.72$ GPa, and the characteristic length in torsion, $\ell_t = 0.94$ mm. This characteristic length is considerably smaller than the cell width 4.5 mm. The goodness of fit was $R^2 = 0.97$. The asymptotic moduli refer to the asymptote at large width. Including fourth order terms has little effect: $G_0 = 0.72$ GPa, $\ell_t = 1.0$ mm, $R^2 = 0.98$. Including theoretical effects of ℓ_b on torsion has little effect on the fits. Fits assuming a small N approximation were poor. The original assumption of N = 1 is thereby supported.

A curve fit (solid curve) for the bending results in the left plot in Figure 4 using Eq. (7) neglecting Poisson's ratio (in view of the anisotropy) revealed the following elastic constants. The inferred asymptotic Young's modulus was $E_0 = 0.92$ GPa, and the characteristic length in bending, $\ell_b = 0.45$ mm. This characteristic length is considerably smaller than the cell width 4.5 mm. The goodness of fit was $R^2 = 0.24$.

A further curve fit (solid curve) was done for the bending results, excluding the low point (right plot in Figure 4). The inferred asymptotic Young's modulus was $E_0=0.94$ GPa, and the characteristic length in bending, $\ell_b=0.48$ mm. This characteristic length is considerably smaller than the cell width 4.5 mm. The goodness of fit was $R^2=0.72$. Including fourth order terms has little effect: $E_0=0.95$ GPa, $\ell_b=0.53$ mm, $R^2=0.69$. Further analyses were done allowing fourth order terms and varying β/γ ; the best results were obtained when $\beta/\gamma=-\nu$ as was initially assumed. Fits in this regime were also insensitive to N.

Comparing torsion and bending, size effects were larger in torsion and the curve fit had a high $R^2 = 0.97$; the bending size effects were less and the fit was highly dependent on the smallest specimen.

The octet truss lattice is considered to be weakly Cosserat elastic with maximum size effects 30% in torsion and 10% in bending, in comparison with foams [17] in which size effects exceeded a factor of 8 in torsion and a factor of 17 in bending, and with designed lattices [18] in which size effects exceeding a factor of 30 were observed.

One might surmise based on experience with a variety of lattices that rib lattices in general [19] will exhibit large nonclassical effects. Indeed, rib lattices designed to exhibit a negative Poisson's ratio [20] or chirality [21] exhibited size effects of a factor of 4.5 and 8 respectively. A simple cubic lattice [21] exhibited size effects of a factor of two in torsion and three in bending. Ribs in the cubic lattice likely exhibited some compliance in bending due to the structure which, due to the high compliance in oblique directions, is not optimal for stiffness. The octet lattice by contrast is triangulated and is stretch dominated for all modes of global deformation. The gyroid lattice which is a stretch-dominated surface lattice exhibited small size effects [22] of less than 20% in its non-chiral form.

The reason for the weak Cosserat effects in the octet lattice is that its behavior is dominated by the stretching of ribs. Cosserat effects depend upon the bending and torsion of the same ribs. The stretch dominated behavior permits a higher elastic modulus at low density than foams because the density dependence of modulus is linear rather than quadratic as it is in foams. By contrast, designed lattices [18] entail bending of substructure within the ribs even when the lattice itself undergoes compression or tension. Similarly, foams have curved ribs that bend under all global deformation conditions. These materials exhibit pronounced Cosserat effects but their ratio of modulus to density is not as high as for stretch dominated cellular solids. Lest one surmise a direct inverse link between optimal stiffness and Cosserat behavior, keep in mind that a composite with stiff particles in a compliant matrix [14] exhibited classical, not Cosserat behavior: $\ell_t = 0$. Homogenization analysis demonstrated that such composites containing stiff spheres have characteristic lengths of zero [23] hence they are classical not Cosserat elastic. Such a composite is the least efficient in terms of stiffness for given concentration of stiff inclusions.

4.4 Comparison with homogenization

No homogenization analysis is available to predict Cosserat effects in the octet truss lattice, however analyses have been done for other rib lattices. Theoretical homogenization of rectangular lattices with straight ribs in 2D [24] was done in the context of Cosserat elasticity. For a square lattice, $\ell = \frac{1}{2} \frac{1}{\sqrt{6}} L_c$ with L_c as the cell size. This is about 0.2 L_c , similar to the observed $\ell_t = 0.17 L_c$. The similarity may be fortuitous in view of the difference in structure. This analytical characteristic length is the ratio of a couple stress term to the lattice shear modulus which, for a square lattice, is much less than Young's modulus in principal directions; the shear modulus of the square lattice depends on bending of ribs.

A body centered model anisotropic configuration in 3D [25] was analyzed but characteristic lengths were not reported. If one divides bend dominated terms that contribute to the couple stress by bend dominated terms that contribute to the axial stress, similarly to the procedure for the above square lattice, a characteristic length is obtained $\ell_1 = \frac{1}{\sqrt{3}}L_c$ with L_c as the cell size. Dividing couple stress terms by stretch dominated terms that contribute to the stress gives $\ell_2 = \frac{1}{\sqrt{3}}w_r$ with w_r as the rib width. Incorporating dimensions for the present lattice (which has a different structure) $\ell_1 = 2.6$ mm and $\ell_2 = 0.3$ mm for the model lattice, compared with experimental values for the octet lattice $\ell_t = 1$ mm and $\ell_b = 0.5$ mm. Observe that for the octet truss lattice and the 3D body centered analytical structure, there are ribs of different length. In view of the complex anisotropy of the 3D model, the meanings of ℓ_1 and ℓ_2 are not obvious. Nevertheless, the observed characteristic lengths of the octet lattice are of the same order of magnitude as the characteristic lengths obtained by homogenization analyses of rib lattices of different structure.

5 Conclusion

The octet truss lattice was observed to exhibit size effects of small magnitude in effective modulus: 30% in torsion and 10% in bending. The lattice is considered to be weakly Cosserat elastic in contrast to prior designed lattices.

6 Acknowledgment

We gratefully acknowledge support by Honeywell Federal Manufacturing and Technologies under Contract No. DE-N000383116 with the U.S. Department of Energy. The United States Government retains and the publisher, by accepting the article for publication, acknowledges that the United States Government retains a nonexclusive, paid up, irrevocable, world-wide license to publish or reproduce the published form of this manuscript, or allow others to do so, for the United States Government purposes.

We also acknowledge partial support by the National Science Foundation via Grant No. CMMI -1906890.

References

- [1] https://www.twi-global.com/what-we-do/research-and-technology/research-reports/industrial-member-re [2] https://www.gknpm.com/globalassets/downloads/additive-manufacturing/datasheets-am-materials/datashe
- [3] https://apps.dtic.mil/dtic/tr/fulltext/u2/a516831.pdf
- H https://www.aubertduval.com/wp-media/uploads/sites/2/2017/06/Ti5553_GB.pdf

- [5] N. Clement, Phase transformations and mechanical properties of the Ti-5553 beta-metastable titanium alloy, page 163. Thesis, Universite catholique de Louvain, Belgium, (2010) https://dial.uclouvain.be/pr/boreal/object/boreal:32266
- [6] G. Gurtner, M. Durand, Stiffest elastic networks, Proc. R. Soc. A: Math. Phys. Eng. Sci., 470, 20130611 (2014).
- [7] T. Tancogne-Dejean, D. Mohr, Elastically-isotropic truss lattice materials of reduced plastic anisotropy, Int. J. Solids Struct., 138, 24-39 (2018).
- [8] Buckminster Fuller, Octahedral building truss, US Patent 3,354,591, (1967).
- [9] V. Deshpande, N. Fleck and M. F. Ashby, Effective properties of the octet truss lattice material, Journal of the Mechanics and Physics of Solids 49, 1747-1769, (2001).
- [10] R. D. Mindlin, Effect of couple stresses on stress concentrations, Experimental Mech., 3, 1-7, (1963).
- [11] Lee, T. Lakes, R. S., and Lal, A. Resonant ultrasound spectroscopy for measurement of mechanical damping: comparison with broadband viscoelastic spectroscopy, Review of Scientific Instruments, 71 (7) 2855-2861, July (2000).
- [12] E. Cosserat, and F. Cosserat, Theorie des Corps Deformables, Hermann et Fils, Paris (1909).
- [13] A. C. Eringen, Theory of micropolar elasticity. In Fracture Vol. 1, 621-729 (edited by H. Liebowitz), Academic Press, New York (1968).
- [14] R. D. Gauthier and W. E. Jahsman, A quest for micropolar elastic constants. J. Applied Mech., 42, 369-374 (1975).
- [15] W. J. Drugan and R. S. Lakes, Torsion of a Cosserat elastic bar with square cross section: theory and experiment, Z. Angew. Math. Phys. 69:24 (2018).
- [16] Lakes, R. S. and Drugan, W. J., Bending of a Cosserat elastic bar of square cross section theory and experiment, Journal of Applied Mechanics (JAM), 82(9), 091002 (2015). (8 pages)
- [17] Z. Rueger and R. S. Lakes, Cosserat elasticity of negative Poisson's ratio foam: experiment, Smart Materials and Structures, 25, 054004 (8pp) (2016).
- [18] Z. Rueger and R. S. Lakes, Strong Cosserat elasticity in a transversely isotropic polymer lattice, Phys. Rev. Lett., **120**, 065501 (2018).
- [19] Rueger, Z., Ha, C. S., and Lakes, R. S., Cosserat elastic lattices, Meccanica, 54(13), 1983-1999, (2019).
- [20] Rueger, Z., Li, D., Lakes, R. S., Observation of Cosserat elastic effects in a tetragonal negative Poisson's ratio lattice, Physica Status Solidi B, 254 (12), 1600840, 6 pages, Dec. (2017).
- [21] Reasa, D. and Lakes, R. S., Cosserat effects in achiral and chiral cubic lattices, Journal of Applied Mechanics (JAM), 86, 111009-1, 6 pages Nov. (2019).
- [22] D. R. Reasa and R. S. Lakes, Nonclassical Chiral Elasticity of the Gyroid Lattice, Phys. Rev. Lett. 125, 205502, 13 November (2020).
- [23] D. Bigoni and W. J. Drugan, Analytical derivation of Cosserat moduli via homogenization of heterogeneous elastic materials, J. Appl. Mech., **74**, 741-753 (2007).
- [24] C. Banks and M. Sokolowski, On certain two dimensional applications of couple stress theory, Int. J. Solids Structures 4, 15-29 (1968).
- [25] T. Tauchert, A lattice theory for representation of thermoelastic composite materials, Recent Adv. Eng. Sci. 5, 325-345, (1970).